

Spin filling and orbital structure of the first six holes in a silicon metal-oxide-semiconductor quantum dot

S. D. Liles¹, R. Li^{1,3}, C. H. Yang², F. E. Hudson², M. Veldhorst^{2,3}, A. S. Dzurak², A. R. Hamilton¹

¹*School of Physics, University of New South Wales, Sydney NSW 2052, Australia*

²*Centre for Quantum Computation and Communication Technology, School of Electrical Engineering and Telecommunications, The University of New South Wales, Sydney NSW 2052, Australia*

³*QuTech and Kavli Institute of Nanoscience, TU Delft, 2600 GA Delft, The Netherlands*

The spin states of electrons confined in semiconductor quantum dots form a promising platform for quantum computation¹⁻³. Recent studies of silicon CMOS qubits have shown coherent manipulation of electron spin states with extremely high fidelity⁴. However, manipulation of single electron spins requires large oscillatory magnetic fields to be generated on-chip, making it difficult to address individual qubits when scaling up to multi-qubit devices^{4,5}. The spin-orbit interaction allows spin states to be controlled with electric fields, which act locally and are easier to generate⁶⁻⁸. While the spin-orbit interaction is weak for electrons in silicon, valence band holes have an inherently strong spin-orbit interaction. However, creating silicon quantum dots in which a single hole can be localised, in an architecture that is suitable for scale-up to a large number of qubits, is a challenge⁹⁻¹². Here we report a silicon quantum dot, with an integrated charge sensor, that can be operated down to the last hole. We map the spin states and orbital structure of the first six holes, and show they follow the Fock-Darwin spectrum^{13,14}. We also find that hole-hole interactions are extremely strong, reducing the two-hole singlet-triplet splitting by 90% compared to the single particle level spacing of 3.5 meV. These results provide a route to single hole spin quantum bits in a planar silicon CMOS architecture.

In this work, we present observations of the first six hole states in a surface-gated silicon metal-oxide-semiconductor quantum dot. Previous studies of planar silicon-based hole quantum dots have used transport measurements to study the addition spectrum of the quantum dot⁹⁻¹¹. However, as these devices approach the few hole regime, the tunnel barriers become extremely opaque, and the transport signal falls precipitously. This has hampered studies of hole quantum dots containing one and two holes, which is the most widely used regime for spin-based quantum computation applications. Figure 1a shows a schematic of the device under study in this letter, and Figure 1b shows a scanning electron microscope image of an identical de-

vice to the one used in this study. The layout of this device is suitable for high frequency spin manipulation experiments⁸, and is optimized for scalability up to many qubits^{15,16}. This device is a hole quantum dot connected to a single reservoir (R) of two-dimensional holes, with an adjacent charge sensor (SHT). By measuring the charge occupation with a charge sensor we are able to study hole states even when the tunnel rate between the dot and reservoir is much smaller than could be detected in transport. In this experiment the number of holes on the dot N is controlled with the bias on gate G3. The dot-reservoir tunnel rate Γ can be tuned without affecting the dot confinement shape using the bias applied to the C-gate.

Hole spins in semiconductor quantum dots are attracting significant attention as candidates for spin-based quantum computation applications^{17,18}, with recent experiments exploiting the strong spin-orbit coupling to demonstrate all-electrical spin manipulation using gate electrodes^{19,20}. Hole spins have the benefit that they are rather insensitive to dephasing induced by hyperfine coupling to the host crystals nuclei-spin^{21,22}. This source of dephasing is the leading cause of decoherence in electron spin qubits²³. Although the effects of hyperfine induced dephasing can be minimized using experimental²⁴ or material⁴ based techniques, the weak coupling of holes to nuclear spins provides the possibility for long coherence times without the need for additional experimental complexity^{25,26}. Further, there is no valley degeneracy in the silicon valence band, avoiding complexities that affect electrons in silicon quantum dots²⁷. Despite these promising properties, hole based quantum dots still face technological challenges that have been overcome in electron systems more than a decade ago³. Demonstrating the ability to isolate one hole and determining the spin properties of the last few holes in surface gated silicon MOS based quantum dots would be a key advance towards realizing hole-spin-based qubits.

In order to characterize the addition spectrum of holes in the quantum dot we employ a pulse-bias technique²⁸, which allows the the charge occupation of the dot to be monitored using an adjacent charge sensor (SHT). We apply a 1mV DC excitation to the SHT's source ohmic contact, and add a continuous square wave of magnitude V_{pulse} and

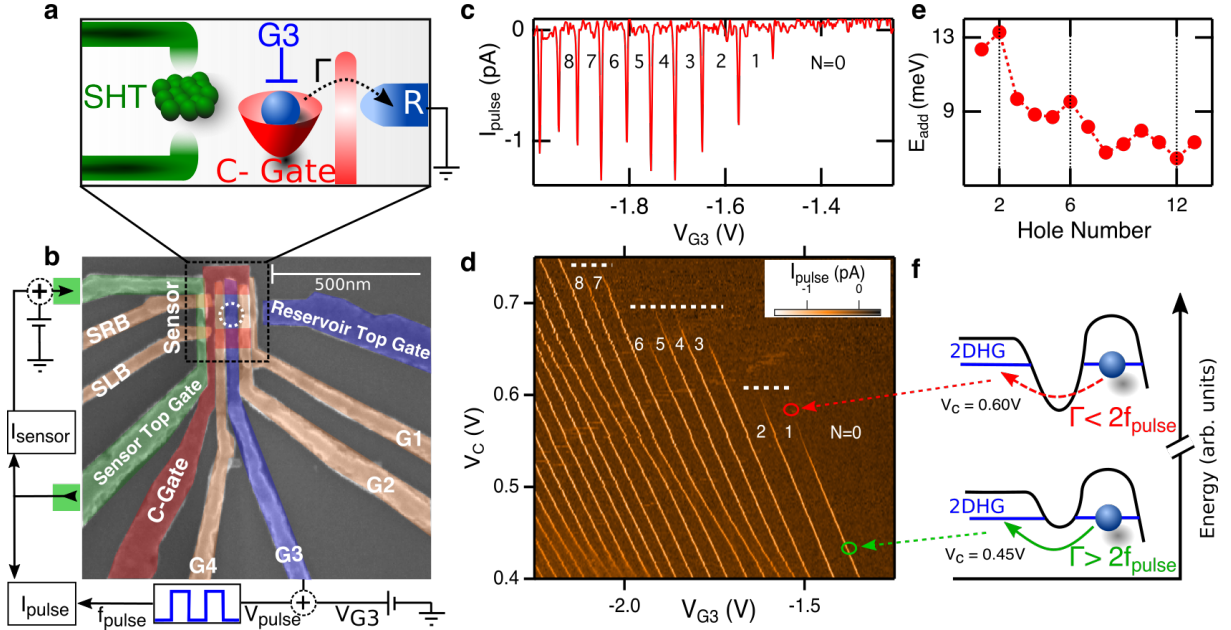


Figure 1: **Silicon quantum dot with charge sensor, capable of reaching the last hole.** **a**, Schematic of the device concept. The device consists of a quantum dot coupled to a single reservoir (R), with an adjacent single hole transistor charge sensor (SHT). The tunnel rate between the dot and reservoir (Γ) can be tuned using the C-gate voltage (V_C), and the dot occupation can be controlled with gate G3 voltage (V_{G3}). **b**, False-coloured scanning electron microscope image of an identical device, with the measurement schematic. **c**, Depletion of the last 10 holes in the quantum dot, showing the V_{pulse} induced signal on the charge sensor measured at $V_C = 0.47V$. **d**, Charge stability diagram, showing the number of holes on the dot as a function of the confining gate and pulse gate potentials. The horizontal white lines highlight the disappearance of the charge transition signals as V_C is increased. The transitions signals disappear in distinct groupings, indicating shell filling. Measurements performed for $V_{pulse} = 3mV$ and $f_{pulse} = 333Hz$. A slight bending in the lines in the vicinity of $(V_{G3} = -2V, V_C = 0.55V)$ is due to coupling to nearby confined charge. **e**, The hole addition energy extracted from **(d)**, showing peaks at $N=2$ and $N=6$ consistent with shell filling. **f**, Schematic diagram showing how the change in the tunnel barrier with V_C causes the charge transition signals to disappear with increasing V_C , when the tunnel time becomes comparable to the length of the pulses applied to gate G3.

frequency f_{pulse} to gate G3. The modulation of the DC sensor current by V_{pulse} , called I_{pulse} , is sensitive to dQ_{dot}/dV_{G3} (as long as $\Gamma > 2f_{pulse}$). In Figure 1c we show a measurement of I_{pulse} as V_{G3} is swept. At specific values of V_{G3} a hole is able to tunnel on and off the dot during the positive/negative phase of V_{pulse} . This charge movement decreases the DC sensor current, causing a negative spike in I_{pulse} of width V_{pulse} in the V_{G3} scan. The measurement of Figure 1c was repeated over a range of V_C to produce the charge stability diagram in Figure 1d. The identification of the last hole in the dot is confirmed by the absence of any additional charge transitions beyond the region labeled $N=0$ in Figure 1d.

The spacing of the charge transition lines in Figure 1d provides clear evidence for orbital shell filling of the hole quantum dot. We extracted the addition energy ($E_{add}(N) = \mu_{N+1} - \mu_N$) by measuring the spacing ΔV_{G3} between consecutive Coulomb peaks, then converted ΔV_{G3} to energy using the lever arm

of $0.17 eV/V$ (see Supporting Information). In Figure 1e we plot the addition energy E_{add} for increasing hole number. A clear increase in the addition energy is observed for $N=2$ and $N=6$, which suggests the orbital shell is full for the second and sixth holes.

Further evidence for orbital shell filling is given by the stair-like disappearance of charge transition signals, which is highlighted by the dashed horizontal white lines in Figure 1d. Along each vertical charge transition line the measured signal decreases as V_C is made more positive. As V_C becomes more positive the tunnel barrier becomes more opaque, and subsequently the tunnel rate from the dot to the reservoir Γ decreases. The charge sensor transition is no longer visible when $\Gamma < 2f_{pulse}$, as shown schematically in Figure 1f. When a hole in the dot occupies a higher energy orbital shell, its wavefunction span increases, which increases the tunnel rate. Hence, the charge sensor transition signals should lose visibility at higher V_C for holes in higher or-

bitals. We observe that the $N=(1,2)$, $(3,4,5,6)$ and $(7,8)$ charge transition lines disappear at the same V_C (dashed lines in Figure 1d), suggesting that these holes fill the same orbital state, with similar tunnel rates in the same orbital level.

These observations of shifts in addition energy and tunnel rate suggest the first two holes fill into the first orbital, and the next four holes fill into the second orbital. This shell filling is consistent with the Fock-Darwin orbital structure for a 2D parabolically confined quantum dot^{13,14}. Beyond $N=6$ the observed orbital filling departs from the so-called 2D magic numbers, which may reflect a loss of circular symmetry of the parabolic confinement for higher hole occupation, or many-body effects²⁹.

To understand the spin structure of the hole quantum dot, we study the magnetic field dependence of the addition energy of the hole dot for $N=1$ to 6 holes. In Figures 2a–e we show the addition energy $\mu_{n+1} - \mu_n$ for the first six holes as a function of in-plane magnetic field B . The slope of the N^{th} addition energy dE_{add}/dB with respect to B depends on the relative spin orientation of the $(N+1)^{\text{th}}$ and N^{th} hole, with three distinct possibilities:

$$\frac{dE_{add}}{dB} = \begin{array}{cc} +g^* \mu_B & \downarrow \uparrow \\ -g^* \mu_B & \uparrow \downarrow \\ 0 & \uparrow \uparrow \text{ or } \downarrow \downarrow \end{array} \quad (1)$$

where the first and second arrow depicts the spin filling sequence of the $(N+1)^{\text{th}}$ and N^{th} holes respectively. We refer to $|B| < 2.7\text{T}$ as the low field region, and $|B| > 2.7\text{T}$ as the high field region. In both the low and high field region of Figures 2a–e the slope dE_{add}/dB is either positive, negative or close to zero, as shown by the dashed lines. Figure 2f shows that the slope of the addition energy for the first six holes in the low field region takes one of three distinct values, consistent with equation 1.

In Figures 2a–e we observe a change in slope at 2.7T. This change in slope suggests a change in the spin filling sequence, which is a result of magnetic field induced orbital level crossings. Knowing the hole number and the relative spin orientations, we can build up the spin shell filling structure in both the low and high field regimes, as indicated in the left and right insets of Figures 2a–e (see Supporting Information).

We now discuss the spin filling sequence in detail, beginning with the low field spin filling. The first and second holes form a Pauli spin pair in a two-fold degenerate orbital, labeled $1s$. The third and fourth holes fill the $2p_x$ and $2p_y$ states with spins parallel to each other. The fifth and sixth holes fill the $2p_x$ and $2p_y$ states with spins parallel to each-other, but opposite to the third and fourth holes.

In Figure 2g we present the hole orbital spectrum extracted from the measurements of E_{add} in

Figures 2a–e. The orbital structure and spin filling for the first six holes is consistent with the expected spin-filling for a parabolically confined two-dimensional quantum dot. The four-fold degeneracy of the $2p_x$ and $2p_y$ orbital levels at $B=0$ demonstrates that the quantum dot has remarkably circular confinement. A key result is the observation of consecutive filling of holes with the same spin orientation ($\downarrow\downarrow$ and $\uparrow\uparrow$), which occurs in the $2p$ orbital. Previous studies of silicon hole quantum dots show only alternating spin filling^{25,30–32}. The results in Figure 2g provide a clear demonstration of the orbital shell spin structure of the first eight holes in a surface-gated silicon quantum dot. In particular, we highlight the observation that holes have spin polarized filling of the $2p$ orbital, analogous to Hund’s first rule of orbital shell filling in atomic physics.

We now discuss the spin filling sequence for $|B| \geq 2.7\text{T}$. The change in slope of $E_{add}(1)$, $E_{add}(2)$ and $E_{add}(3)$ at $B=2.7\text{T}$ can be attributed to a magnetic field induced crossing of the $1s$ and $2p$ orbitals, as shown in Figure 2g). We have extracted the orbital effective g-factors g^* from Figure 2f to be $g_{1s}^* = 1.08$ and $g_{2p}^* = 1.39$. By calculating the Zeeman energy at the $1s$ and $2p$ crossing we determine the singlet-triplet energy spacing E_{ST} for the two hole dot is 0.2meV.

The change in slope around 2.7T for $E_{add}(4)$ and $E_{add}(5)$ can be attributed to a crossing between the $2p$ orbital and the next highest orbital level. The next highest orbital level above the $2p$ orbital is two-fold degenerate and is occupied by the 7^{th} and 8^{th} holes (Figure 2g). For circular 2D confinement the orbital level above $2p$ is expected to be six-fold degenerate. We suspect that the two-fold degenerate orbital above the $2p$ orbital may be result from a loss of circular symmetry of the dot due to for higher hole occupations, or many body effects²⁹.

To further study the orbital shell structure, and the nature of the confinement potential we examined the excited state spectrum of the quantum dot. Figure 3a shows the charge stability diagram when V_{pulse} is increased to 40mV. Increasing V_{pulse} broadens the charge transition window, allowing single hole tunneling to occur via either the ground state or an excited state. The excited state spectrum can be resolved by observing the additional structure of I_{pulse} within broadened charge transition lines.

Figure 3b shows the excited state spectrum for the dot with single hole occupation. This spectrum is obtained from a high resolution cut of I_{pulse} vs. V_{G3} along the dashed white line labeled (b) in Figure 3a. The x-axis in Figure 3b is converted to energy using the lever arm (see Supporting Information) and the ground state is set to zero energy. Peaks in Figure 3b correspond to the single hole tunneling into different orbital states in the unoccupied quantum dot ($0 \rightarrow 1$ transition).

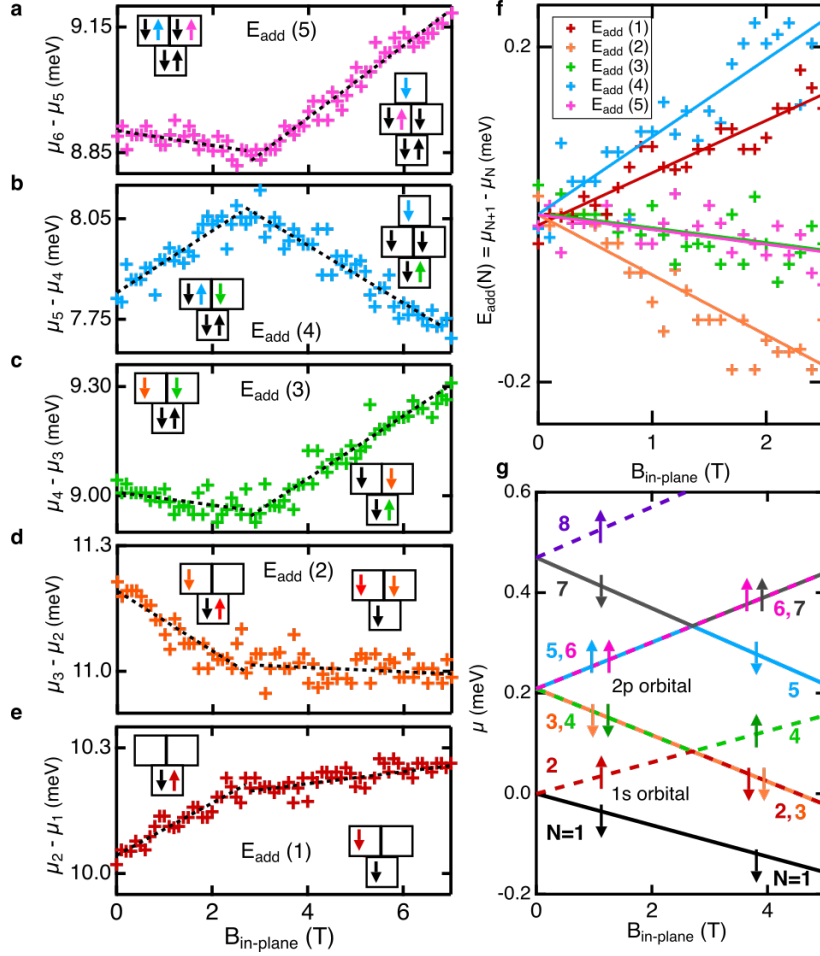


Figure 2: **Spin filling sequence and orbital structure.** a-e, Addition energy for the first 6 holes as a function of in-plane magnetic field. The black dashed line is a linear fit to the raw data over the region $|B| < 2.7\text{T}$ (low field) and $|B| > 2.7\text{T}$ (high field). The left and right inset shows the inferred ground state spin filling for the low and high magnetic field regions respectively. f, The addition energies of (a)-(e) plotted over the low field region with data offset to clarify the three distinct slopes, positive, negative, and close to zero. Solid lines are least squares fit to the data. g, Model of the hole orbital shell structure for the first eight holes (ignoring Coulomb charging energy), which explains the observed addition energies in (a)-(e). The colours of the orbitals correspond to the hole charge occupations in (a)-(e).

The extracted orbital energies are plotted as black circles in Figure 3d, and show a linear dependence on orbital number. This linearity implies a remarkably parabolic confinement potential. We note that additional structure can be observed in I_{pulse} for the second excited state (ES2) and the third excited state (ES3) in Figure 3b. This additional structure is likely due to orbital splitting resulting from ellipticity of the dot for higher energy orbitals, consistent with results in Figure 1d.

We now estimate the expected excited state energy scales in order to compare with the experiment. The quantum dot radius was calculated to be $\sim 27\text{nm}$, by approximating the dot as a parallel plate capacitor and using the charging energy of 12meV for the one to two hole charge occupation. A dot radius of 27nm is smaller than previous silicon MOS hole quantum dots operating in the few

hole regime^{10,11,33}. The expected orbital spacing for a 2D artificial atom with 27nm radius is $\sim 3\text{meV}$, which is consistent with the measured orbital spectrum in Figure 3d.

Finally, we investigated the energy spectrum of the two hole quantum dot. We can determine the strength of hole-hole interactions within the quantum dot by comparing the two-hole energy spectrum with the one-hole energy spectrum. Figure 3c shows the excited state spectrum for the two-hole quantum dot, which is a cut along the dashed white line labeled (c) in Figure 3a. A key feature of the two hole dot is that the first excited state is now only 0.25meV above the ground state (inset of Figure 3c), while the separation between excited states remains comparable to the $N=1$ transition excited state energy separation of $\sim 3\text{meV}$. The reduction in the spacing between the ground state and

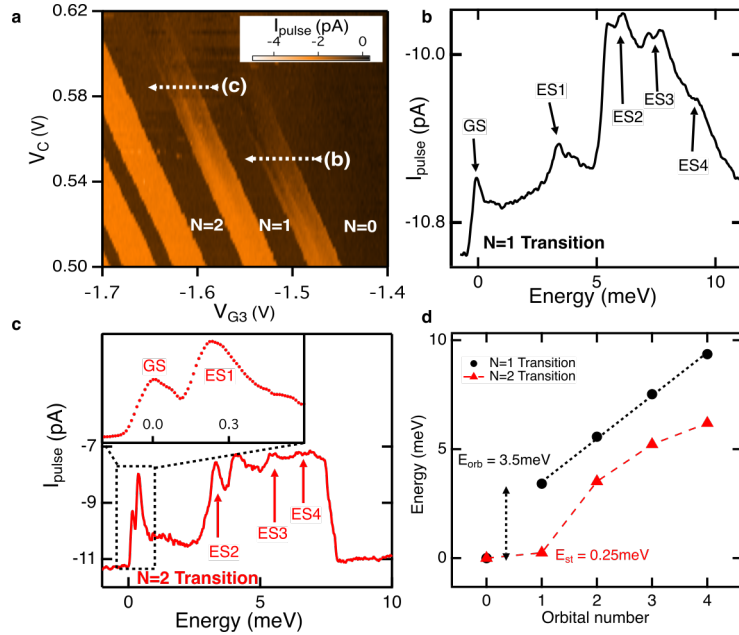


Figure 3: **Excited state spectroscopy.** **a**, Charge stability diagram for $V_{pulse} = 40\text{mV}$ and $f_{pulse} = 333\text{Hz}$. The white dashed lines labelled (b) and (c) correspond to cut taken to obtain the data in **b** and **c** respectively. **b**, Measurement of I_{pulse} over the $N=0 \rightarrow 1$ Coulomb peak. The x-axis has been converted to energy using the lever arm (Supporting Information S). The ground state (GS) and excited states (ES1-4) for the one hole system are labelled. Additional structure is observed for ES2 and ES3, see text. **c**, Same as (b) for the $N=1 \rightarrow 2$ Coulomb peak. The inset demonstrates that the ground state and first excited state are resolvable. Each dot represents a single data point. **d**, Plot of the extracted excited state energies for the one (black) and two (red) hole system. The black dashed line is a straight line fit to the $N=1$ data for orbital number ≥ 1 , highlighting the linear dependence of the excited state energies on the orbital number.

first orbital state (3.5meV for the one hole system, and 0.25meV for the two hole system) results from the additional Coulomb interaction energy when one hole already occupies the lowest energy orbital. The observation of a 0.25meV excited state spacing for the two-hole dot is consistent with the 0.2meV Zeeman energy required to induce a singlet-triplet ground state transition in Figure 2e. Based on the change in first orbital energy spacing, we estimate that the hole interaction energy is $\sim 90\%$ of the orbital energy, which is much larger than in electron systems^{27,28}. This large interaction energy has significant implications for Pauli spin blockade and quantum information applications.

In summary, we have demonstrated a silicon MOS based quantum dot operating in the last hole regime. The orbital level spacing demonstrates that the confinement potential is remarkably parabolic. We have extracted the ground state spin filling for $N=1$ to 8 holes. The spin shell filling for the first six holes is found to be consistent with predictions for a circular 2D quantum dot. Finally, we determine that strong hole-hole interactions affect the two-hole energy spectrum, resulting in suppression of the singlet-triplet energy spacing. These results highlight the unique physics of 2D hole artificial

atoms, and clearly demonstrate that spin properties and energy scales are very different to nanowire and electron artificial atoms^{3,25,30,31}.

Methods

The Sample: The device studied in this work was fabricated using a high resistivity natural (001) silicon substrate. The P+ ohmic regions are prepared by boron diffusion. A 5.9nm gate dielectric (SiO_2) is grown by dry oxidation in the active region of the device. The gate pattern is fabricated using multilayer Al- Al_2O_3 gate stack technology³³. The final stage is a forming gas (95% N_2 /5% H_2) anneal to reduce Si/ SiO_2 interface disorder and enhance low temperature performance. All measurements were performed in a dilution fridge with a base temperature below 30mK.

When operating the device, the reservoir top gate is negatively biased to accumulate a 2D hole system at the Si/ SiO_2 interface below. The quantum dot is defined by positively biasing gates G1, G2, G4, and the C-gate. G3 acts as the dot plunger gate and is operated in the negatively biased regime. It is possible to operate this device in the double dot regime down to the (0,0) charge state, using gate G2 as the second dot's plunger gate. Additionally, in the double dot regime we can observe inter-dot tunneling. See Supporting information for more information on the tunability of this device.

Charge Sensor: The pulse-bias charge sensing method has been extensively described in Refs. [27,28]. In order to maximize the sensitivity of the charge sensor we use a feedback loop on the sensor gate to keep the sensor at the same conductance as the other gates are swept, as described in Ref. [34]. We note that the charge transitions signals using I_{pulse} in Figure 1d are sensitive to the dot tunnel rate, hence we have also confirmed the charge occupation by simultaneously measuring the sensor conductance using I_{sensor} , which is not sensitive to the tunnel rate. See the Supporting Information for full details.

Magneto-spectroscopy: In order to infer the spin con-

figuration of the dot for different hole occupations we measure the spin state of all additional holes relative to the first hole, which we assume is aligned with the in-plane magnetic field B . The $N=1$ spin ground state is assigned as down. The relative spin orientation of the first six holes can be inferred from the data presented in Figures 2a-e, and is well described by the orbital model presented in Figure 2d). Further discussion regarding the spin filling of the 7th and 8th holes is provided in the Supporting Information.

Pulse-bias spectroscopy: The charge stability diagram shown in Figure 3a is obtained using the same gate bias configuration as the stability diagram in Figure 1b, except the charge transitions are broader due to increased V_{pulse} . When sweeping V_{G3} over a broadened charge transition signal (as indicated by the horizontal dashed lines in Figure 3a), I_{pulse} initially increases as the ground state is pulsed below the reservoir electrochemical potential μ_{res} . I_{pulse} then decays as V_{G3} becomes more negative, since the effective tunnel barrier increases. For sufficiently negative V_{G3} additional excited states become accessible for tunneling, which increases the tunnel rate and causes additional spikes in I_{pulse} .

References

- Daniel Loss and David P DiVincenzo. Quantum computation with quantum dots. *Physical Review A*, 57(1):120, 1998.
- Ronald Hanson, Leo P Kouwenhoven, Jason R Petta, Seigo Tarucha, and Lieven MK Vandersypen. Spins in few-electron quantum dots. *Reviews of Modern Physics*, 79(4):1217, 2007.
- Floris A Zwanenburg, Andrew S Dzurak, Andrea Morello, Michelle Y Simmons, Lloyd CL Hollenberg, Gerhard Klimeck, Sven Rogge, Susan N Coppersmith, and Mark A Eriksson. Silicon quantum electronics. *Reviews of modern physics*, 85(3):961, 2013.
- M Veldhorst, JCC Hwang, CH Yang, AW Leenstra, Bob de Ronde, JP Dehollain, JT Muhonen, FE Hudson, KM Itoh, A Morello, et al. An addressable quantum dot qubit with fault-tolerant control-fidelity. *Nature nanotechnology*, 9(12):981–985, 2014.
- FHL Koppens, Christo Buizert, Klaas-Jan Tielrooij, IT Vink, KC Nowack, Tristan Meunier, LP Kouwenhoven, and LMK Vandersypen. Driven coherent oscillations of a single electron spin in a quantum dot. *Nature*, 442(7104):766–771, 2006.
- Vitaly N Golovach, Massoud Borhani, and Daniel Loss. Electric-dipole-induced spin resonance in quantum dots. *Physical Review B*, 74(16):165319, 2006.
- Christian Flindt, Anders S Sørensen, and Karsten Flensberg. Spin-orbit mediated control of spin qubits. *Physical review letters*, 97(24):240501, 2006.
- KC Nowack, FHL Koppens, Yu V Nazarov, and LMK Vandersypen. Coherent control of a single electron spin with electric fields. *Science*, 318(5855):1430–1433, 2007.
- Ruoyu Li, Fay E Hudson, Andrew S Dzurak, and Alexander R Hamilton. Pauli spin blockade of heavy holes in a silicon double quantum dot. *Nano letters*, 15(11):7314–7318, 2015.
- Paul C Spruijtenburg, Joost Ridderbos, Philipp Mueller, Anne W Leenstra, Matthias Brauns, Antonius AI Aarnink, Wilfred G van der Wiel, and Floris A Zwanenburg. Single-hole tunneling through a two-dimensional hole gas in intrinsic silicon. *Applied physics letters*, 102(19):192105, 2013.
- Yu Yamaoka, Kazuma Iwasaki, Shunri Oda, and Tetsuo Kodera. Charge sensing and spin-related transport property of p-channel silicon quantum dots. *Japanese Journal of Applied Physics*, 56(4S):04CK07, 2017.
- AC Betz, MF Gonzalez-Zalba, G Podd, and AJ Ferguson. Ambipolar quantum dots in intrinsic silicon. *Applied Physics Letters*, 105(15):153113, 2014.
- Vladimir Fock. Bemerkung zur quantelung des harmonischen oszillators im magnetfeld. *Zeitschrift für Physik A Hadrons and Nuclei*, 47(5):446–448, 1928.
- Charles Galton Darwin. The diamagnetism of the free electron. In *Mathematical Proceedings of the Cambridge Philosophical Society*, volume 27, pages 86–90. Cambridge University Press, 1931.
- Eric Dennis, Alexei Kitaev, Andrew Landahl, and John Preskill. Topological quantum memory. *Journal of Mathematical Physics*, 43(9):4452–4505, 2002.
- Cody Jones, Mark F Gyure, Thaddeus D Ladd, Michael A Fogarty, Andrea Morello, and Andrew S Dzurak. A logical qubit in a linear array of semiconductor quantum dots. *arXiv preprint arXiv:1608.06335*, 2016.
- P Szumniak, S Bednarek, B Partoens, and FM Peeters. Spin-orbit-mediated manipulation of heavy-hole spin qubits in gated semiconductor nanodevices. *Physical review letters*, 109(10):107201, 2012.
- Christoph Kloeffel, Mircea Trif, Peter Stano, and Daniel Loss. Circuit qed with hole-spin qubits in ge/si nanowire quantum dots. *Physical Review B*, 88(24):241405, 2013.
- VS Pribiag, S Nadj-Perge, SM Frolov, JWG Van Den Berg, I Van Weperen, SR Plissard, EPAM Bakkers, and LP Kouwenhoven. Electrical control over single hole spins in nanowire quantum dots. *arXiv preprint arXiv:1302.2648*, 2013.
- R Maurand, X Jehl, D Kotekar-Patil, A Corna, H Bohuslavskiy, R Laviéville, L Hutin, S Barraud, M Vinet, M Sanquer, and Silvano De Franceschi. A cmos silicon spin qubit. *Nature communications*, 7:13575, 2016.
- Denis V Bulaev and Daniel Loss. Spin relaxation and anti-crossing in quantum dots: Rashba versus dresselhaus spin-orbit coupling. *Physical Review B*, 71(20):205324, 2005.
- ZK Keane, MC Godfrey, JCH Chen, S Fricke, O Klochan, AM Burke, AP Micolich, HE Beere, DA Ritchie, KV Trunov, et al. Resistively detected nuclear magnetic resonance in n- and p-type gaas quantum point contacts. *Nano letters*, 11(8):3147–3150, 2011.
- FHL Koppens, KC Nowack, and LMK Vandersypen. Spin echo of a single electron spin in a quantum dot. *Physical review letters*, 100(23):236802, 2008.
- Lorenza Viola and Seth Lloyd. Dynamical suppression of decoherence in two-state quantum systems. *Physical Review A*, 58(4):2733, 1998.
- Yongjie Hu, Ferdinand Kuemmeth, Charles M Lieber, and Charles M Marcus. Hole spin relaxation in ge-si core-shell nanowire qubits. *Nature nanotechnology*, 7(1):47–50, 2012.
- Andrew P Higginbotham, Thorvald Wadum Larsen, Jun Yao, Hao Yan, Charles M Lieber, Charles M Marcus, and Ferdinand Kuemmeth. Hole spin coherence in a ge/si heterostructure nanowire. *Nano letters*, 14(6):3582–3586, 2014.
- CH Yang, WH Lim, NS Lai, A Rossi, A Morello, and AS Dzurak. Orbital and valley state spectra of a few-electron silicon quantum dot. *Physical Review B*, 86(11):115319, 2012.
- JM Elzerman, R Hanson, LH Willems van Beveren, LMK Vandersypen, and LP Kouwenhoven. Excited-state spectroscopy on a nearly closed quantum dot via charge detection. *Applied physics letters*, 84(23):4617–4619, 2004.
- M Ciorga, AS Sachrajda, Pawel Hawrylak, C Gould, Piotr Zawadzki, S Jullian, Y Feng, and Zbigniew Wasilewski. Addition spectrum of a lateral dot from coulomb and spin-blockade spectroscopy. *Physical Review B*, 61(24):R16315, 2000.
- Stefano Roddaro, Andreas Fuhrer, Patrik Brusheim, Carina Fasth, HQ Xu, Lars Samuelson, J Xiang, and CM Lieber. Spin states of holes in ge/si nanowire quantum dots. *Physical review letters*, 101(18):186802, 2008.
- Floris A Zwanenburg, Cathalijn EWM van Rijmenam, Ying Fang, Charles M Lieber, and Leo P Kouwenhoven. Spin states of the first four holes in a silicon nanowire quantum dot. *Nano letters*, 9(3):1071–1079, 2009.

32. Matthias Brauns, Joost Ridderbos, Ang Li, Erik PAM Bakkers, and Floris A Zwanenburg. Electric-field dependent g-factor anisotropy in ge-si core-shell nanowire quantum dots. *Physical Review B*, 93(12):121408, 2016.
33. Ruoyu Li, Fay E Hudson, Andrew S Dzurak, and Alexander R Hamilton. Single hole transport in a silicon metal-oxide-semiconductor quantum dot. *Applied Physics Letters*, 103(16):163508, 2013.
34. CH Yang, WH Lim, FA Zwanenburg, and AS Dzurak. Dynamically controlled charge sensing of a few-electron silicon quantum dot. *AIP Advances*, 1(4):042111, 2011.

Acknowledgments

This work was funded by the Australian Research Council (CE11E0001017 and DP150100237) and the US Army Research Office (W911NF-13-1-0024). Devices were made at the NSW node of the Australian National Fabrication Facility. We thank D. Miserev, O. Sushkov, and D. Q. Wang for helpful discussions.

Author Contributions

S.D.L and R.L performed the experiments and F.E.H and M.V fabricated the device. R.L, S.D.L, C.H.Y, and A.R.H designed the experiments. S.D.L and R.L analyzed the results and S.D.L, R.L, C.H.Y, A.S.D and A.R.H contributed to discussions. S.D.L wrote the manuscript with help from all co-authors.

Additional Information

The authors have provided Supporting Information that contains the following details; A confirmation of absolute charge occupation of the dot, independent of the tunnel rate; Tuning the dot to reservoir tunnel rate and operation of the device as a double quantum dot; Lever arm and hole temperature calculation; and Spin filling of the 7th and 8th holes.

Competing financial interests

The authors declare no competing financial interests.